RESEARCH ARTICLE

STABILITY AND OPTICAL PROPERTIES OF VANADIUM WITH GGA AND GGA+U CALCULATIONS

Yousif Shoaib Mohammed[*1,2,3,4], **Ahmed Faisal Ahmed**[5], **Abd Elmoniem A. Elzain**[1,6], **Arafa A. Yagob**[7], **Elnoor Abbakar Abdelrahman Noh**[8,9] **and Khidir Shaib Mohamed**[10,11]

[1]Department of Physics, College of Science & Art, Qassim University, Oklat Al-Skoor, P.O. Box: 111, Saudi Arabia; [2]Department of Physics, College of Education, Dalanj University, Dalanj, Sudan; [3]Department of Science, College of Aviation Sciences, Karary University, PortSudan – Sudan; [4]Department of Physics, Africa City for Technology, Khartoum, Sudan; [5]Department of Physics, College of Science, Qassim University, Buraidah, P.O. Box 6666, Saudi Arabia; [6]Department of Physics, University of Kassala, Kassala, P.O.Box: 266, Sudan; [7]Department of Physics, Jazan University, Saudi Arabia; [8]Faculty of Science and arts in Baljurashi, Al-Baha University, Saudi Arabia; [9]Department of Chemistry, College of Education, Dalanj University, Dalanj, Sudan; [10]Department of Mathematic, College of Science & Art, Qassim University, Oklat Al-Skoor, P.O.Box: 111, Saudi Arabia; [11]Department of Mathematic and Computer, College of Science, Dalanj University, Dalanj, Sudan

ARTICLE INFO

ABSTRACT

The stability of the bcc non-magnetic (NM) state in Vanadium (V) and the optical properties are investigated, using the full-potential linearized augmented plane wave (FP-LAPW) method with the generalized gradient approximation (GGA) and GGA+U within the framework of density functional theory (DFT), as implemented in the WIEN2k computational package code. As compared to other 3d transition metals such as Fe, Co, and Ni, the non-magnetic state of bcc V has been found to be distinct from that seen in previous studies. We have discovered that the density of state (DOS), for both GGA and GGA+U, doesn't change much with NM and AFM states, however the DOS differs significantly with FM states. The lowest partial density of state (PDOS) at EF is for FM with GGA+U, while the maximum PDOS is for NM with GGA+U. In addition, the d-states of V contribute to the DOS's valence band maximum (VBM). In terms of the optical properties, we computed the interband dielectric function $\varepsilon(\omega)$, variation in the energy-loss spectrum $L(\omega)$, absorption coefficient $\alpha(\omega)$, refractive index $n(\omega)$, reflectivity $R(\omega)$, and optical absorption $\sigma(\omega)$ for bcc V for NM, FM, and AFM states. We discovered that our results were comparable and superior to those of the other studies.

INTRODUCTION

Despite the large number of experimental and theoretical studies conducted for a deeper understanding of the nature of optical properties and magnetism in 3d transition metals under ambient conditions, stability as well as optical and magnetic properties of 3d transition elements remain some of the most fundamental questions in solid-state physics [1,2,11–13]. For elemental bcc vanadium, chromium, manganese, and iron, the transition from nonmagnetic to ferromagnetic behavior has been investigated [14] by examining self-consistent parameter-free total energy band structure calculations in the local spin density approximation (LSDA) using a fixed-spin-moment method. In our earlier work [2], we used the Vienna ab initio simulation package (VASP) to investigate the stability of

ferromagnetism in Fe, Co, and Ni metals under high pressure using GGA and GGA+U. Additionally, using a self-consistent theory of the electronic structure, the Fermi-surface, optical, and photoemission properties of copper are provided [15]. Furthermore, Akoh, H. and A. Tasaki [16] used the evaporation method prepared hyperfine particles (100 to 1000) of vanadium, and the magnetic susceptibility of these tiny particles was measured between 1.6 and 300 K. While, Langridge-Smith, et al. [17] using the first gas-phase electronic spectra, reported the band length and electronic structure of V2. In this study, we used GGA and GGA+U computations with the WIEN2k code [18,19], to examine the stability, DOS, and optical properties of vanadium. Vanadium is a metal in group VB of the periodic table with an atomic weight of 50.94, an atomic number of 23, and a density of 6.1 mg/m^3 [20]. It has atomic radius of 0.134 nm, and a melting temperature of 1900 °C. Vanadium has a body centered cubic crystal structure at room temperature, with one atom per lattice point. Experimentally, the properties of 3d transition metals have been investigated in many ways. Paolo A. Sossi et al [21] have been

*Corresponding author: *Yousif Shoaib Mohammed*
Department of Physics, College of Science & Art, Qassim University, Oklat Al-Skoor, P.O. Box: 111, Saudi Arabia

used piston cylinder experiments to study the calibration of vanadium partitioning and stable isotope fractionation between hydrous granitic melt and magnetite at 800 °C and 0.5 GPa. Moreover, Laser vaporization of vanadium metal generated the bond length and electronic structure of V2 in an expansion-cooled molecular beam. A strong band structure with an origin close to 7000 Å was observed using the technique of resonant two photon ionization spectroscopy [17]. Additionally, hyperfine particles (100 to 1000 Å) of vanadium were prepared by the evaporation method and the magnetic susceptibility of these fine particles was measured in the temperature range between 1.6 to 300 K [16]. Furthermore, the properties of Fe are taken into account across its 2p core levels, where it is shown that the resonant atomic scattering factor in the electric dipole approximation and the general equivalence of classical magneto-optical formalism dielectric tensor can both describing the pure charge contributions as well as first and second order magnetic contributions [22]. From a theoretical perspective, the self-consistent-field molecular-orbital theory and density-functional approximation were used to study magnetism in tiny vanadium clusters [1]. They demonstrated that if vanadium's size and dimensions were constrained, it may become magnetic. Both linear chains and vanadium clusters with body-centered-cubic (bcc) of vanadium influence observed this behavior. They also discovered that, the clusters in linear-chain configurations always maintain their moment, while the magnetic moment of the bcc clusters abruptly disappears as size increases. Additionally, using the energy values and wave functions determined by the APW method in the energy range 0-40 eV, the complex dielectric function $\varepsilon(0, \omega)$ and energy-loss function $-Im[\varepsilon(0, \omega)-1]$ of the 3d transition metals (V, Cr, Fe, and Ni) are computed within RPA [12]. On the other hand, Sanyal B. et al. [23] show that V, Cr, and Mn compounds exhibit half metallic behavior for appropriate lattice constants. They have determined that the ferromagnetic phase is more stable than the antiferromagnetic one by comparing their total energies. The Cr-based systems show the greatest interatomic exchange interactions for the different compounds studied. In the other side, the APW method has been used to compute the X-ray form factors for metallic vanadium [24]. Using ratios of the integrated X-ray scattering intensities for reflection pairs, the charge asphericity are computed having the same value of sin (theta/lambda). While, Wakoh S. et al. [25] using the wave functions derived by the APM method, computed the compton profiles by caused to the band electrons in vanadium and chromium.

METHODS

The density of state (DOS), optical properties, and ground state energy for Vanadium (V) per formula unit for non-magmetic, ferromagnetic, and antiferromagnetic states have all been calculated in this work using the full-potential linearized augmented plane wave (FP-LAPW) method [26] based on density functional theory (DFT) [27] as implemented in WIEN2k computational package code [18,19,28,29]. In the Perdew-Burke-Ernzerhof (PBE) approach[30], the exchange correlation interaction was treated within the Generalized Gradient Approximation (GGA) for each case. In the atomic sphere, the wave function is extended into atomic-like functions (radial functions times spherical harmonics), and in the interstitial region, it is expressed in terms of a plane wave basis. It is widely known that the experimental band gap is often underestimated by the GGA approximation [31]. In order to take into account the electronic correlation, we use a rotationally invariant DFT+U version proposed by Dudarev et al. [32]. The parameters U and J in this method represent on-site Coulomb interaction energy and exchange energy, respectively. Only their difference, *U-J*, was meaningful; the parameters *U* and *J* were not used separately. The GGA+*U* details are shown in Refs. [33]. We utilize (U-J) = 2.3 eV, taken from [34], in GGA+U calculations for our V phases. This value is quite similar to *U* = 3.1 eV for V [35–37], where the exchange energy parameter is set to the typical value of *J* = 1 eV. For Brillouin zone sampling, the Monkhorst-Pack scheme [38,39] is used. The irreducible Brillouin zone contains 1000 as number of k points, with $R_{MT} \times K_{max}$ = 7.50 for well-converged results, where K_{max} is the plane wave cut-off. The term Gmax, which is used to indicate the magnitude of the largest

wave vector in charge density, is considered to taken a value of 12.00. The cut-off energy and charge convergence criteria allow for up to 0.0001e charge in successive iterations [40]. The integration across the Brillion zone was carried out using the linear tetrahedron approach with Blochl corrections for calculations of total energy and DOS [41,42]. The Murnaghan equations of state (EOS) [43–48] were fitted to the calculated total energies as functions of volume to obtain the equilibrium volume V_o, the zero-pressure bulk modulus B_o, and its pressure derivatives B_o'.

RESULTS AND DISCUSSION

Structure Properties: The computed total energy (atomic energy) as a function of the unit cell volume for bcc and fcc V metal in the NM, FM, and AM phases with the GGA and GGA+*U*, respectively, is shown in Figures1 and 2. These figures showed us that the non-magnetic bcc structure is the ground state of V for both approximations. Our findings were consistent with earlier studies [1,49]. According to the GGA and GGA+*U*, Table 1 shows the computed equilibrium atomic volume V_o, lattice constant *a*, and atomic energy *E* at equilibrium volume for each phase. This also ensured that the results of the GGA and GGA+*U* calculations correctly predicted that the ground state would be an NM bcc structure, which is consistent with the findings of earlier investigations [50,51]. According to Table 1, the atomic volume for bcc V decreases when strong correlations are taken into account, whereas fcc V exhibits oscillating behaviour. Additionally, it is clear from this table that the bcc V gives quite reasonable results that are rather realistic when compared to those of other 3d elements, such as those from our earlier work for Stability of Ferromagnetism in Fe, Co, and Ni Metals under High Pressure with GGA and GGA+*U* [2].
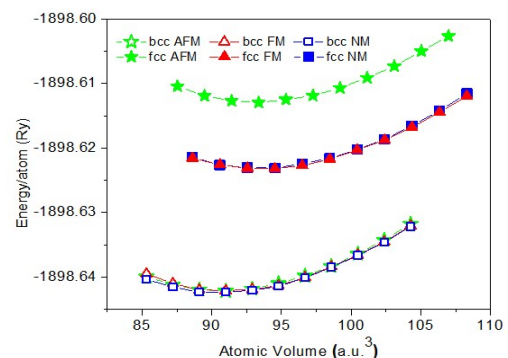

Figure 1. (Online color) Calculated total energies as a function of the atomic volume for V with Muraghan EOS; blue cube for NM; red triangle for FM and green star for AFM with GGA calculations, open symbols for bcc and solid symbols for fcc states, respectively
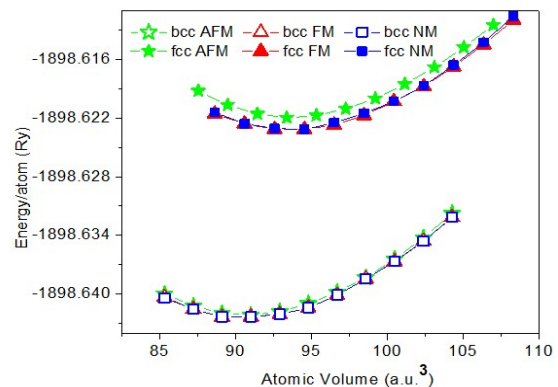

Figure 2. (Online color) Calculated total energies as a function of the atomic volume for V with Muraghan EOS; blue cube for NM; red triangle for FM and green star for AFM with GGA+*U* calculations, open symbols for bcc and solid symbols for fcc states, respectively

Table 1. Calculated atomic volume V_0, lattice constant a, and atomic energy E for NM, FM, and AFM states for bcc and fcc V phases with Murnaghan EOS, with GGA and GGA+U, respectively. (The calculated results by GGA+U are in parenthesis)

Case	V_o (a.u.^{3})	a (A^o)	E (Ry)
bcc V NM	90.555(90.533)	2.994(2.994)	-1898.6424 (-1898.6424)
bcc V FM	90.978(90.567)	2.999(2.994)	-1898.6422 (-1898.6424)
bcc V AFM	90.655(90.647)	2.995(2.995)	-1898.6421 (-1898.6421)
fcc V NM	93.453(93.491)	3.812(3.813)	-1898.6231 (-1898.6231)
fcc V FM	93.461(93.457)	3.812(3.812)	-1898.6232 (-1898.6232)
fcc V AFM	93.175(93.542)	3.808(3.813)	-1898.6129 (-1898.6219)

Table 2.Calculated atomic volume V_o, bulk modulus B_o, and bulk modulus pressure derivative B_o', for NM, FM, and AFM states of bcc and fcc V by GGA and GGA+U, respectively, together with experimental data and previous calculated results (The calculated results by GGA+U are in parenthesis)
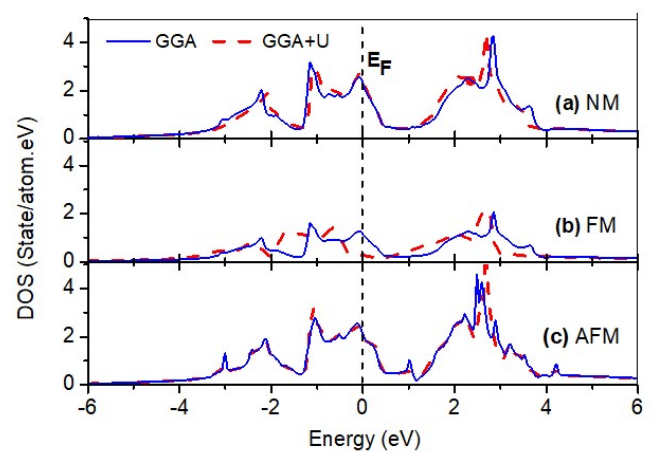
Case	Method	Type	V_o (a.u.^{3})	B_o (GPa)	B_o'	Reference
bcc V NM	DFT	GGA (GGA+U)	90.555(90.533)	184.893 (182.982)	4.019(3.858)	This work
bcc V FM	"	"	90.978(90.567)	200.415 (185.597)	4.797(4.029)	"
bcc V AFM	"	"	90.655(90.647)	185.228 (184.894)	3.581(3.561)	"
bcc V	WHM	-	-	160	5.81	[53]
bcc V	-	-	-	-	4.26	[54]
bcc V	-	-	-	-	4.69	[55]
bcc V	-	-	-	-	4.53	[56]
bcc V	-	-	-	-	3.451	[57]
fcc V NM	DFT	GGA (GGA+U)	93.453(93.491)	177.784 (178.566)	3.246(3.315)	This work
fcc V FM	"	"	93.461(93.457)	179.905 (179.883)	3.976(3.978)	"
fcc V AFM	"	"	93.175(93.542)	189.326 (184.578)	4.371(4.498)	"

Table 2 lists the results of the ground-state properties, including the equilibrium volume V_o, zero pressure bulk modulus B_o, and its pressure derivative B_o', together with any available experimental information and earlier all-electron calculations. According to Table 2, the atomic volume for bcc decreases when strong correlations are taken into account, but the atomic volume for fcc changes oscillatorily. Additionally, it is evident from this table that the GGA provides findings that are pretty realistic when compared to other results [52–56]. So, compared to previous DFT results, the GGA results exhibit a significant improvement, i.e., better agreement with experiments and other theoretical investigations.

Electronic properties

We report the total density of state TDOS and partial density of state PDOS of NM, FM, and AFM using GGA and GGA+U calculations, respectively, as shown in Figures3, 4, 5, and 6 for the states of various phases NM, FM, and AFM to investigate the correlation between magnetic phase and the electronic structure, which explains the energy levels of bcc V. Energy levels between -6 and 6 eV have been reported for the calculations. The vertical dotted line in our calculated DOS denotes the energy level, or Fermi level. Figure 3 shows that while the DOS shape does not significantly change with the NM and AFM states, it does significantly change with the FM state. Iota's experiments [57] and associated theoretical studies [2,3,12] are compatible with this. It is well known that the stoner criteria for an itinerant is given by N(EF)>1, where N(EF) is the DOS at the Fermi level (EF) and I is the Stoner parameter. For our study phases, this criterion is satisfied, however it is not satisfied for FM with

GGA+U.Figure 3, also show that the Fermi levels of NM and AFM are mainly contributed by the e_g level. Additionally, it may be understood by taking into account the contributions that the addition of U and J made to the Stoner parameter, I [34,36].

Figure 3 (Online color) Calculated TDOS of bcc V (a) NM, (b) FM, and (c) AFM,solid and dashed curves represent the GGA and GGA+U, respectively

Figures 4, 5, and 6 illustrate the calculations of PDOS of the s, p, d, and f states, for the NM, FM, and AFM phases of the bcc V with GGA and GGA+U, respectively. Our result that an antiferromagnetic

ordering removes the instability caused by the high density of states at Fermi energy, is in excellent agreement with that reported in Ref [58], For all of our examples, the V:3d orbitals are primarily responsible for the maximum amount of energy in the range between 2.73 and 2.98 eV. Additionally, it is clear from these figures that the *d* orbital has the highest state density. According to the cases we studied, and in line with what M. Junaid et al. [59] reported, d-states of V have the least impact on the valence band maximum (VBM) for *s* and *f*-states. Additionally, PDOS plots show the *p-d* hybridization, and it is clear that the represent of the Hubbard term changes the local positions of the states by contrasting the distribution of DOS under GGA and GGA+*U*. The V states move lower as a result of the addition of *U*, weakening the V 3d hybridization. For NM and AFM with GGA and GGA+*U*, the impurity states close to the Fermi level stay essentially the same, however for FM, the GGA+*U* calculation appears to be different with the lowest energy at the Fermi level. According to table 3, the PDOS at EF is highest for NM with GGA+*U* and lowest for FM with GGA+*U*.

Figure 6. (Online color) Calculated Local DOS of AFM bcc V (a) GGA and (b) GGA+*U*. Solid, dot, dash dot, dash and dash dot dot, for total, *s*, *p*, *d* and *f* DOS, respectively

Table 3. Calculated the DOS at Fermi energy E_F for NM, FM and AFM states of bcc V by GGA and GGA+*U*, respectively. (The calculated results by GGA+*U* are in parenthesis)

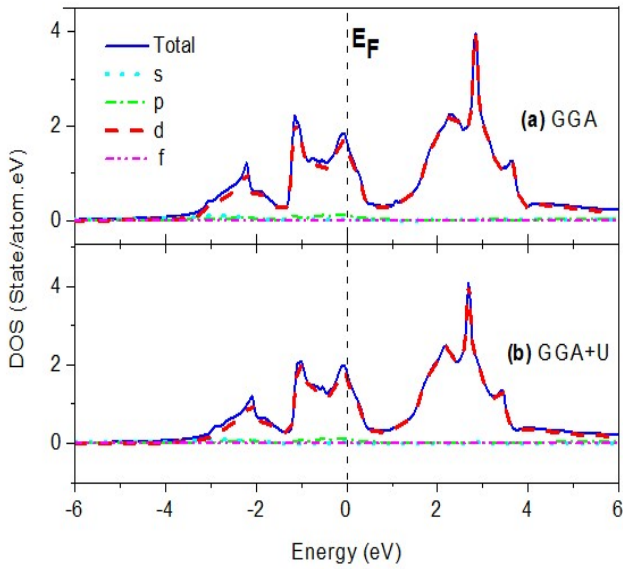| Case	DOS at E_F
NM	2.49 (2.65)
FM	1.24 (0.28)
AFM	2.04 (2.22)

Figure 4. (Online color) Calculated PDOS of NM bcc V (a) GGA and (b) GGA+*U*. Solid, dot, dash dot, dash and dash dot dot, for total, *s*, *p*, *d* and *f* DOS, respectively
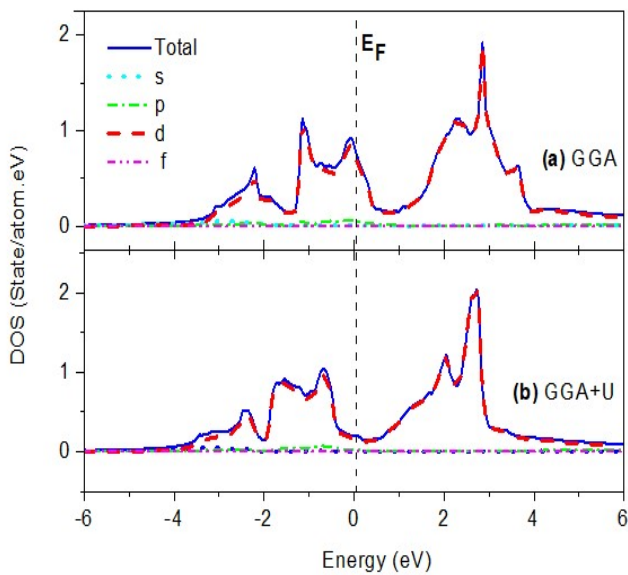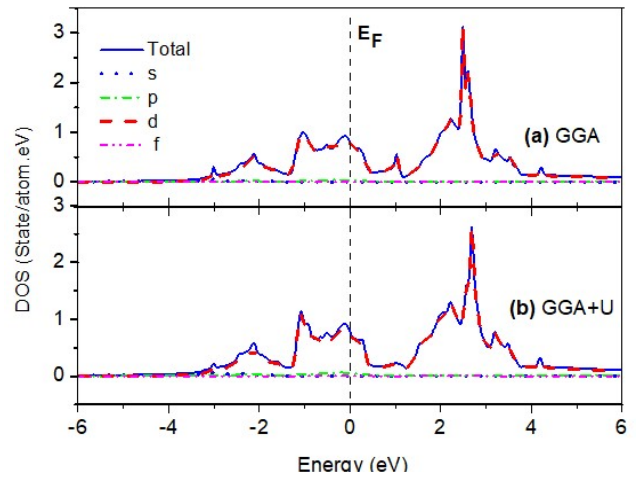
Optical Properties: Numerous studies have been done on the optical properties [12,13,60,61]. The band structures that are described by the inter/intra band transitions are closely related to the optical properties. The interaction of an incident photon with atoms is regarded as a material's optical response, and it can be described by the dielectric function $\varepsilon(\omega)$. The crystal is considered as an isotrope for a cubic symmetry structure $\left(\varepsilon = \varepsilon_{xx} = \varepsilon_{yy} = \varepsilon_{zz}\right)$. It is known that the interband dielectric function $\varepsilon(\omega)$ determines the physical properties of solids and describes the optical response of the medium at all photon energy. The dielectric function $\varepsilon(\omega)$ has two parts, real part $\varepsilon_1(\omega)$ and imaginary part $\varepsilon_2(\omega)$, given as [62].

$$\varepsilon(\omega) = \varepsilon_1(\omega) + i\varepsilon_2(\omega) \qquad \text{………………..(1)}$$

The Kramers-Kronig relations [63] provide the real and imaginary parts $\varepsilon_1(\omega)$, $\varepsilon_2(\omega)$ of the complex dielectric function $\varepsilon(\omega)$ respectively, which is directly related to the electronic band structure and describes the absorptive behavior.

$$\varepsilon_1(\omega) = 1 + \frac{2}{\pi}P\int_0^\infty \frac{\omega'\varepsilon_2(\omega')}{\left(\omega'^2 - \omega^2\right)}d\omega' \qquad \text{………………(2)}$$

$$\varepsilon_2(\omega) = \frac{2\omega}{\pi}P\int_0^\infty \frac{\varepsilon_1(\omega')-1}{\left(\omega'^2 - \omega^2\right)}d\omega' \qquad \text{………………...(3)}$$

where ω is the incident photons frequency, and P is the Cauchy integral main part. All other optical parameters can be easily derived, when $\varepsilon_1(\omega)$ and $\varepsilon_2(\omega)$ are determined, i.e., absorption coefficient $\alpha(\omega)$, refractive indices $n(\omega)$, energy loss function $L(\omega)$, and reflectivity $R(\omega)$. Previous Computing of optical properties occurred [64–66]. The interband dielectric function $\varepsilon(\omega)$, computed using FP-LAPW for the NM, FM, and AFM states of bcc V, is shown in Figures 7 and 8 for the real part $\varepsilon_1(\omega)$ and imaginary part $\varepsilon_2(\omega)$. The values of the $\varepsilon_1(\omega)$ and $\varepsilon_2(\omega)$ for the NM and AFM states are

Figure 5.(Online color) Calculated PDOS of FM bcc V (a) GGA and (b) GGA+*U*. Solid, dot, dash dot, dash and dash dot dot, for total, *s*, *p*, *d* and *f* DOS, respectively

computed in these figures for the energy range of 0 to 13 eV with GGA and GGA+U and for FM with GGA+U, whereas the calculations are done for the energy range of 0 to 0.7 eV for FM with GGA. We found from these figures that our $\varepsilon_1(\omega)$ and $\varepsilon_2(\omega)$ behaviorin an arrangement that is typically consistent with experimental and theoretical investigations [3-6]. The figures for our bcc study cases with GGA and GGA+U calculations all exhibit oscillatory behavior, with the exception of FM with GGA, which exhibits strange smooth behavior for changing $\varepsilon_1(\omega)$ and $\varepsilon_2(\omega)$ with energy. Table 3 includes a list of the main peak locations located for $\varepsilon_2(\omega)$. The results of earlier studies [4,5] are easily supported by this table and figures 7 and 8, which show that all peaks altered oscillatory with increasing energy and various numbers of peaks for every situation. For FM with GGA, the shift was smooth. Figure 8 shows that for NM, FM, and AFM with GGA (GGA+U), the shoulders occur at 2.75(2.71), (2.6), and 2.32(2.5) eV, respectively. Behind this, as seen in figures 4-6 of PDOS for our bcc examples, one can observe that the main contribution to $\varepsilon_2(\omega)$ comes from the most d-DOS.
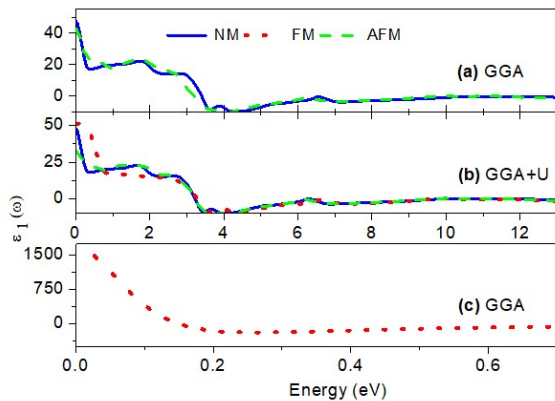

Figure 7. (Online color) Calculated real part $\varepsilon_1(\omega)$ of the dielectric function for NM, FM and AFMstates (a) and (b) between 0 and 13 eV and (c) between 0 and 0.7 eV with GGA and GGA+U, respectively
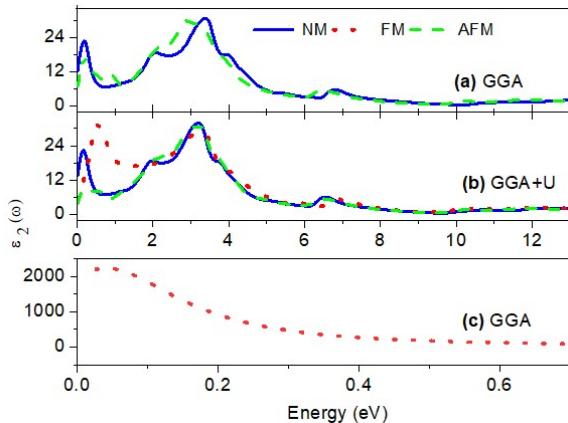

Figure 8. (Online color) Calculated Imaginary part $\varepsilon_2(\omega)$ of the dielectric function for NM, FM and AFM states(a) and (b) between 0 and 13 eV and (c) between 0 and 0.7 eV with GGA and GGA+U, respectively

Table 4. Calculated the main peaks points of the imaginary part $\varepsilon_2(\omega)$ of the dielectric functionfor NM, FM and AFM states of bcc V by GGA and GGA+U, respectively. (The calculated results by GGA+U are in parenthesis).

NM	FM	AFM
0.18 (0.18)	(0.54)	0.19 (0.19)
2.01 (1.93)	(3.25)	0.93 (0.54)
3.40 (3.19)	(6.87)	2.15 (2.19)
6.85 (6.50)	-	2.93 (3.19)
-	-	6.50 (6.46)

Figure 9, show the variation in the energy-loss spectrum $L(\omega)$ for NM, FM, and AFM with both GGA and GGA+U calculations, respectively. The considered concentrations in this figure are plotted in the energy range of 0–13 eV, for all cases of study except for FM with GGA, where the energy range is 0–0.7 eV. Because $\varepsilon_2(\omega)$ has significant energy value [7], we noticed that these spectra display minimum values. For NM, FM, and AFM with GGA and GGA+U, the main peaks are located at 10.37(9.84), (9.71), and 9.66(9.71) eV; respectively (GGA+U calculations are in parenthesis). These values and graph behavior are comparable to previous investigations [7-9]. Additionally, part (c) of this figure demonstrates how the FM GGA calculation behaves differently and strangely from all other cases with a smooth graph shape and no peak.
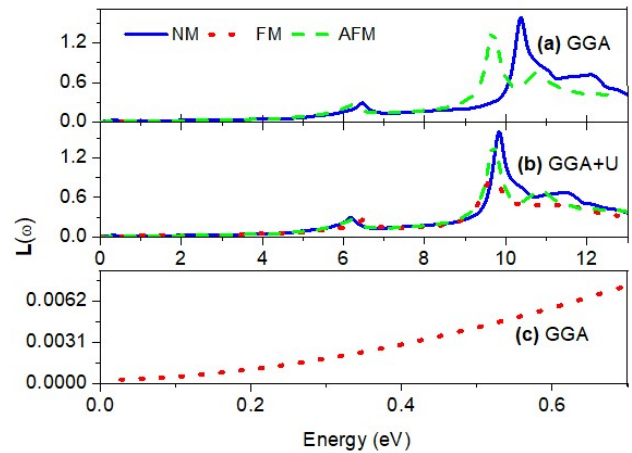

Figure 9. (Online color) Calculated energy loss function $L(\omega)$ for NM, FM and AFM states(a) and (b) between 0 and 13 eV and (c) between 0 and 0.7 eV with GGA and GGA+U, respectively

The results for the absorption coefficient $\alpha(\omega)$ are displayed in Figure 10. In this figure, parts (a) and (b), show the results for NM, FM, and AFM using both the GGA and GGA+U calculations from 0 to 13 eV of bcc V, whereas part (c) shows the results for only FM using the GGA, from 0 to 0.7 eV, respectively. According to this figure, the optical absorption is activated for NM, FM, and AFM with GGA and GGA+U at 0.24(0.12), 0.05(0.30), and 0.008(-0.074) eV, respectively (the results for GGA+U are in parenthesis). The results we obtained in this figures are extremely in line with other studies [10,12].
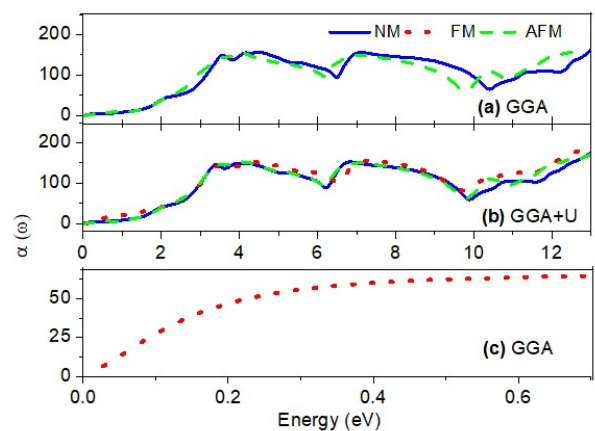

Figure 10. (Online color) Calculated absorption coefficient $\alpha(\omega)$ for NM, FM and AFM states(a) and (b) between 0 and 13 eV and (c) between 0 and 0.7 eV with GGA and GGA+U, respectively

Figure 11 displays the fluctuations in the refractive index $n(\omega)$ as a function of energy for various states of bcc V. Results for NM, FM, and AFM with both GGA and GGA+U

are shown at (a) and (b), respectively, from 0 to 13 eV, while results for only FM with GGA are shown at (c), from 0 to 0.7 eV. Table 5 shows the greatest peak energy for Figure 11. This figure and table 5 showed us that our results' behavior was consistent with those of other studies [67, 68].
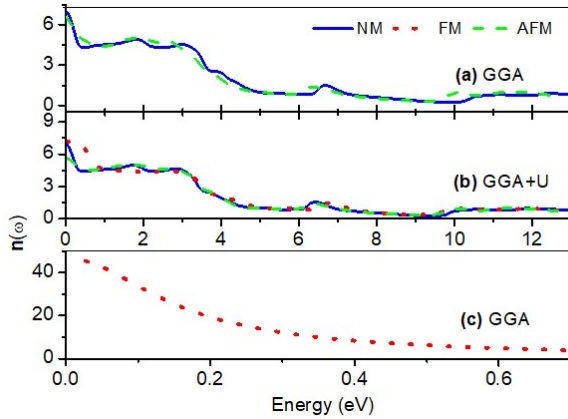

Figure 11. (Online color) Calculated the refractive index *n(w)* for NM, FM and AFM states(a) and (b), between 0 and 13 eV and (c), between 0 and 0.7 eV with GGA and GGA+*U*, respectively.

Table 5. Calculated maximum peaks energies of refractive index *n(w)* for NM, FM and AFM states of bcc V by GGA and GGA+*U*, respectively. (The results calculated by GGA+*U* are in parenthesis)

NM	FM	AFM
1.81 (1.74)	(2.68)	0.81 (1.81)
3.12 (2.93)	(6.82)	1.87 (2.68)
6.69 (6.56)	(10.07)	3.06 (6.38)
11.20 (10.20)	(11.95)	6.32 (10.14)
12.52 (12.39)	-	11.71 (11.77)

Figure 12 shows the reflectivity $R(\omega)$ for various states as a function of energy. The results were shown at (a) and (b), from 0 to 13 eV of bcc V for NM, FM, and AFM with both GGA and GGA+*U*, whereas our result was shown at (c), from 0 to 0.7 eV for only FM with GGA. For NM, FM, and AFM with GGA and GGA+*U*, the maximum peak energies appear at 3.56(3.37), 0.09(3.60), and 3.47(3.42), respectively. (The calculated results by GGA+*U* are in parenthesis).
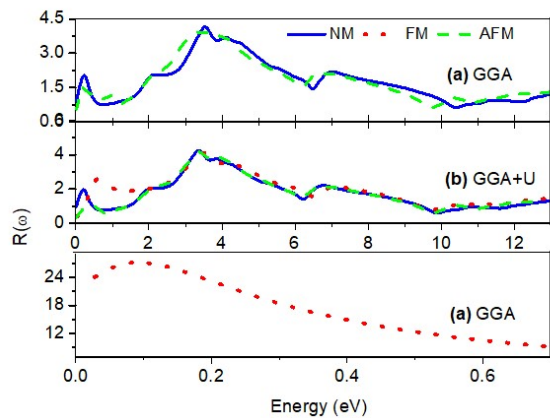

Figure 12. (Online color) Calculated the reflectivity *R(ω)* for NM, FM and AFM states,(a) and (b), between 0 and 13 eV and (c), between 0 and 0.7 eV with GGA and GGA+*U*, respectively

The greatest peak energies of the reflectivity $R(\omega)$ of figure 12 for our study's cases are displayed in Table 6. Figure 12 and Table 6 showed that our results behaved in a manner that was consistent with earlier studies [69].

Table 6. Calculated the maximum peaks energies of reflectivity *R(ω)* for NM, FM and AFM states of bcc V by GGA and GGA+*U*, respectively. (The calculated results by GGA+*U* are in parenthesis)

NM	FM	AFM
0.23 (0.18)	0.10 (0.68)	0.18 (0.49)
3.56 (3.31)	(3.56)	0.89 (3.37)
4.12 (3.88)	(7.19)	3.47 (6.88)
7.03 (6.76)	(10.64)	6.80
11.11 (10.95)	-	10.95 (10.39)

The fluctuation of the optical absorption $\sigma(\omega)$, real and imaginary parts $\sigma_1(\omega)$ and $\sigma_2(\omega)$, are displayed in Figures13 and 14, respectively. The significant photon energy absorption of real part $\sigma_1(\omega)$ of the optical absorption peaks are seen in figure 13, in the range of (0.14-13.00) eV for (a) and (b), and from (0.026-0.70) eV for (c), which is consistent with the imaginary part $\varepsilon_2(\omega)$ of the dielectric function. The imaginary parts $\sigma_2(\omega)$ of the optical absorption peaks displayed in figure 14. It shows strong absorption of the photon energy in the range of (0.14-13.00) eV for (a) and (b), and from (0.026-0.70) eV for (c), which also in consistent with $\varepsilon_2(\omega)$.
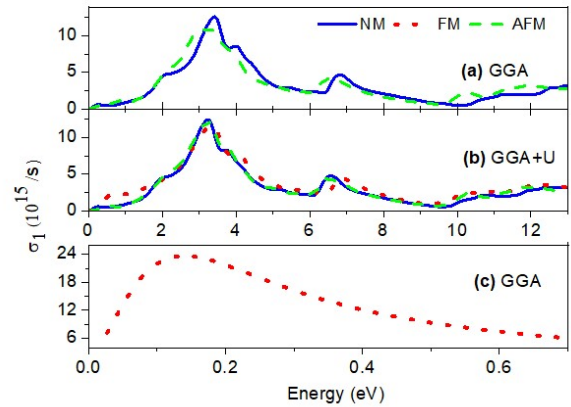

Figure 13. (Online color) The variation of optical conductivity real part *σ₁(ω)* for NM, FM and AFM states, (a) and (b), between 0 and 13 eV and (c), between 0 and 0.7 eV with GGA and GGA+*U*, respectively

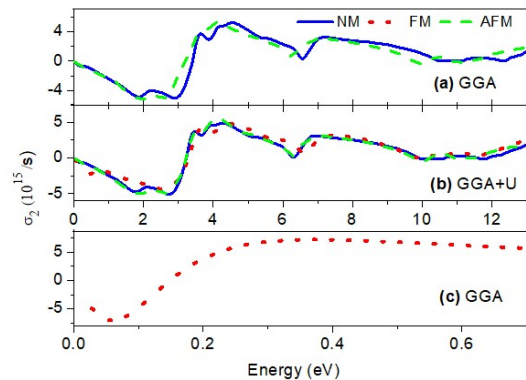**Figure 14. (Online color) The variation of optical conductivity imaginary part *σ₂(ω)*for NM, FM and AFM states, (a) and (b), between 0 and 13 eV and (c), between 0 and 0.7 eV with GGA and GGA+*U*, respectively**

DISCUSSION

This study presents the following conclusions in summary:

(1) It is found that the stability of non-magnetic state of bcc V agrees with previous study [1], is very different for other 3d transition metals [2], and is closely associated with the crystal structure.

(2) Calculated results suggest to possibility that the NM state of bcc V can be transition to antiferromagnetic under ambit conditions, due to the previous study results, i.e., the stability of ferromagnetism in Fe, Co, and Ni metals under high pressure [2,11] and to the similarity behavior of the NM and AFM states. However the FM state is quite different.

(3) For GGA and GGA+U, we found no discernible difference in the total densities of states (DOS) between NM and AFM states; however the DOS significantly varies with FM state. Additionally, NM with GGA+U has the highest partial density of state (PDOS) at EF, while FM with GGA+U has the lowest PDOS. Moreover, the valence band maximum (VBM) for the DOS is influenced by the d-states of V.

(4) The obtained results for optical properties, such as the interband dielectric function $\varepsilon(\omega)$, variation in the energy-loss spectrum $L(\omega)$, absorption coefficient $\alpha(\omega)$, refractive index $n(\omega)$, reflectivity $R(\omega)$, and optical absorption $\sigma(\omega)$ for bcc V for NM, FM, and AFM states are similar to those of other studies [3-10].

REFERENCES

[1] Liu, F., S. Khanna, and P. Jena, Magnetism in small vanadium clusters. Physical Review B. 43 (1991) 8179.

[2] Mohammed, Y.S., et al., Stability of ferromagnetism in Fe, Co, and ni metals under high pressure with GGA and GGA+ U. Journal of magnetism and magnetic materials. 322 (2010) 653-657.

[3] Laurent, D., C. Wang, and J. Callaway, Energy bands, Compton profile, and optical conductivity of vanadium. Physical Review B. 17 (1978) 455.

[4] Johnson, P.B. and R.-W. Christy, Optical constants of the noble metals. Physical review B. 6 (1972) 4370.

[5] Johnson, P. and R. Christy, Optical constants of transition metals: Ti, v, cr, mn, fe, co, ni, and pd. Physical review B. 9 (1974) 5056.

[6] Nestell Jr, J. and R. Christy, Optical conductivity of bcc transition metals: V, Nb, Ta, Cr, Mo, W. Physical Review B. 21 (1980) 3173.

[7] Dadsetani, M. and A. Pourghazi, Optical properties of strontium monochalcogenides from first principles. Physical Review B. 73 (2006) 195102.

[8] Misell, D. and A. Atkins, Electron-energy loss spectra for the first transition series. Philosophical Magazine. 27 (1973) 95-106.

[9] Marton, L., Experiments on low-energy electron scattering and energy losses. Reviews of Modern Physics. 28 (1956) 172.

[10] Romaniello, P., et al., Optical properties of bcc transition metals in the range 0–40 eV. Physical Review B. 73 (2006) 075115.

[11] Ishimatsu, N., et al., Stability of ferromagnetism in Fe, Co, and Ni metals under high pressure. Journal of the Physical Society of Japan. 76 (2007) 064703-064703.

[12] Kubo, Y. and S. Wakoh, Optical Properties of 3d Transition Metals: V, Cr, Fe and Ni. Journal of the Physical Society of Japan. 50 (1981) 835-842.

[13] Weaver, J., D.W. Lynch, and C. Olson, Optical properties of V, Ta, and Mo from 0.1 to 35 eV. Physical Review B. 10 (1974) 501.

[14] Moruzzi, V., P. Marcus, and P. Pattnaik, Magnetic transitions in bcc vanadium, chromium, manganese, and iron. Physical Review

B. 37 (1988) 8003.

[15] Janak, J., A. Williams, and V. Moruzzi, Self-consistent band theory of the Fermi-surface, optical, and photoemission properties of copper. Physical Review B. 11 (1975) 1522.

[16] Akoh, H. and A. Tasaki, Appearance of magnetic moments in hyperfine particles of vanadium metal. Journal of the Physical Society of Japan. 42 (1977) 791-795.

[17] Langridge-Smith, P.R., et al., The bond length and electronic structure of V2. The Journal of chemical physics. 80 (1984) 593-600.

[18] Blaha, P., et al., wien2k. An augmented plane wave+ local orbitals program for calculating crystal properties. 60 (2001).

[19] Blaha, P., et al., WIEN2k, An Augmented Plane Wave Plus Local Orbitals Program for Calculating Crystal Properties (Vienna University of Technology, Austria, 2001). Google Scholar There is no corresponding record for this reference, 2002.

[20] Callister, W., Materials Science and Engineering: An Introduction 4th edition John Wiley and Sons. Inc., London, (1997).

[21] Sossi, P.A., J. Prytulak, and H.S.C. O'Neill, Experimental calibration of vanadium partitioning and stable isotope fractionation between hydrous granitic melt and magnetite at 800 C and 0.5 GPa. Contributions to mineralogy and petrology. 173 (2018) 1-18.

[22] Kortright, J.B. and S.-K. Kim, Resonant magneto-optical properties of Fe near its 2 p levels: Measurement and applications. Physical Review B, 2000. **62**(18): p. 12216.

[23] Sanyal, B., L. Bergqvist, and O. Eriksson, Ferromagnetic materials in the zinc-blende structure. Physical Review B. 68 (2003) 054417.

[24] Wakoh, S. and Y. Kubo, Charge asphericity in vanadium metal. Journal of Physics F: Metal Physics. 10 (1980) 2707.

[25] Wakoh, S., Y. Kubo, and J. Yamashita, Compton Profiles due to the Band Electrons in Metallic Vanadium and Chromium. Journal of the Physical Society of Japan. 40 (1976) 1043-1047.

[26] Petersen, M., et al., Improving the efficiency of FP-LAPW calculations. Computer Physics Communications. 126 (2000) 294-309.

[27] Bagayoko, D., Understanding density functional theory (DFT) and completing it in practice. AIP Advances. 4 (2014) 127104.

[28] Tran, F., WIEN2k: an augmented plane wave plus local orbitals program for calculating crystal properties.(2018).

[29] Schwarz, K., P. Blaha, and G.K. Madsen, Electronic structure calculations of solids using the WIEN2k package for material sciences. Computer physics communications. 147 (2002) 71-76.

[30] Zhang, Z., Y. Sun, and R.M. Wentzcovitch, PBE-GGA Predicts the B8 $\leftrightarrow$ B2 Phase Boundary of FeO at Earth's Core Conditions. arXiv preprint arXiv:2211 (2022) 15052.

[31] Johnson, K.A. and N. Ashcroft, Corrections to density-functional theory band gaps. Physical Review B. 58 (1998) 15548.

[32] Dudarev, S.L., et al., Electron-energy-loss spectra and the structural stability of nickel oxide: An LSDA+ U study. Physical Review B. 57 (1998) 1505.

[33] Hendrik J. Monkhorst and James D. Pack, Special points for Brillouin-zone integrations. Phys. Rev. B. 13 (1976) 5188.

[34] Wang, Q.-B., et al., A GGA+ U study of the optical properties of vanadium doped ZnO with and without single intrinsic vacancy. Optics Communications. 297 (2013) 79-84.

[35] Jain, A., et al., Formation enthalpies by mixing GGA and GGA+ U calculations. Physical Review B. 84 (2011) 045115.

[36] Aykol, M. and C. Wolverton, Local environment dependent GGA+ U method for accurate thermochemistry of transition metal compounds. Physical Review B. 90 (2014) 115105.

[37] Wang, L., T. Maxisch, and G. Ceder, Oxidation energies of transition metal oxides within the GGA+ U framework. Physical Review B. 73 (2006) 195107.

[38] Monkhorst, H.J. and J.D. Pack, Special points for Brillouin-zone integrations. Physical review B. 13 (1976) 5188.

[39] Pack, J.D. and H.J. Monkhorst, " Special points for Brillouin-zone integrations"—a reply. Physical Review B. 16 (1977) 1748.

[40] Mustafa, G., et al., Electronic and magnetic properties of BaUO3 by modified Becke–Johnson (mBJ) functional. Modern Physics Letters B. 32 (2018) 1850164.

[41] Methfessel, M. and A. Paxton, High-precision sampling for Brillouin-zone integration in metals. Physical Review B. 40 (1989) 3616.

[42] Blöchl, P.E., Projector augmented-wave method. Physical review B. 50 (1994) 17953.

[43] Birch, F., The effect of pressure upon the elastic parameters of isotropic solids, according to Murnaghan's theory of finite strain. Journal of Applied Physics. 9 (1938) 279-288.

[44] Birch, F., Finite elastic strain of cubic crystals. Physical review. 71 (1947) 809.

[45] Murnaghan, F.D., The compressibility of media under extreme pressures. Proceedings of the National Academy of Sciences. 30 (1944) 244-247.

[46] Vinet, P., et al., Universal features of the equation of state of solids. Journal of Physics: Condensed Matter. 1 (1989) 1941.

[47] Tarantola, J.P.A., A logarithmic equation of state. Phys. Earth Planet. Inter. 109 (1998) 1.

[48] Poirier, J.-P. and A. Tarantola, A logarithmic equation of state. Physics of the Earth and Planetary Interiors. 109 (1998) 1-8.

[49] Moruzzi, V., Singular volume dependence of transition-metal magnetism. Physical review letters. 57 (1986) 2211.

[50] Hattox, T.M., et al., Calculation of the magnetization and total energy of vanadium as a function of lattice parameter. Journal of Physics and Chemistry of Solids. 34 (1973) 1627-1638.

[51] Moruzzi, V. and P. Marcus, Magnetism in bcc 3 d transition metals. Journal of applied physics. 64 (1988) 5598-5600.

[52] Raju, S., E. Mohandas, and V. Raghunathan, The pressure derivative of bulk modulus of transition metals: An estimation using the method of model potentials and a study of the systematics. Journal of Physics and Chemistry of Solids. 58 (1997) 1367-1373.

[53] Batsanov, S.S., Effects of explosions on materials: modification and synthesis under high-pressure shock compression. (1994): Springer Science & Business Media.

[54] Rose, J.H., et al., Universal features of the equation of state of metals. Physical Review B. 29 (1984) 2963.

[55] Freund, J. and R. Ingalls, Inverted isothermal equations of state and determination of B0, B'0 and B0. Journal of Physics and Chemistry of Solids. 50 (1989) 263-268.

[56] Walzer, U., Calculations of the Hugoniot pressure and pressure derivative of the bulk modulus for transition metals. High Temperatures. High Pressures (Print). 19 (1987) 161-176.

[57] Iota, V., et al., Electronic structure and magnetism in compressed 3 d transition metals. Applied Physics Letters. 90 (2007) 042505.

[58] Saoud, F.S., J.C. Plenet, and M. Henini, Band gap and partial density of states for ZnO: Under high pressure. Journal of Alloys and Compounds. 619 (2015) 812-819.

[59] Khan, M.J.I., et al., Investigating structural, electronic and optical properties of CdS: Cr (A GGA and GGA+ U study). Solid State Sciences. 108 (2020) 106437.

[60] Rai, D., et al., Electronic and optical properties of cubic SrHfO3 at different pressures: a first principles study. Materials Chemistry and Physics. 186 (2017) 620-626.

[61] Yamashita, J., Y. Kubo, and S. Wakoh, Optical Properties of Mo and Nb Calculated from APW Band Structures. Journal of the Physical Society of Japan. 42 (1977) 1906-1913.

[62] Ajmad, I., B. amin, M. Maqbool, S. Muhammad, G. Murtaza, S. Ali, A. Noor. Chin. Phys. Lett. 29 (2012) 097102.

[63] Wooten, F., Optical Properties of Solids Academic Press: New York. NY, USA, London, UK. (1972).

[64] Delin, A., et al., Optical properties of the group-IVB refractory metal compounds. Physical Review B. 54 (1996) 1673.

[65] Bekhti-Siad, A., et al., Electronic, optical and thermoelectric investigations of Zintl phase AE3AlAs3 (AE= Sr, Ba): first-principles calculations. Chinese journal of physics. 56 (2018) 870-879.

[66] Behera, D., et al., Electronic, optical, and thermoelectric investigations of Zintl phase AAg2Se2 (A= Sr, Ba) compounds: A first-principle approach. Journal of Solid State Chemistry. 312 (2022) 123259.

[67] Currie, M., M.A. Mastro, and V.D. Wheeler, Characterizing the tunable refractive index of vanadium dioxide. Optical Materials Express. 7 (2017) 1697-1707.

[68] Wan, C., et al., On the optical properties of thin-film vanadium dioxide from the visible to the far infrared. Annalen der Physik. 531 (2019) 1900188.

[69] Cormier, P., et al., Vanadium dioxide as a material to control light polarization in the visible and near infrared. Optics Communications. 382 (2017) 80-85.

****